https://doi.org/10.5194/acp-2022-756
Preprint. Discussion started: 23 December 2022

Atmospheric Chemistry and Physics Discussions

A view of the European carbon flux landscape through the lens of the ICOS atmospheric observation network

Ida Storm[1], Ute Karstens[1], Claudio D'Onofrio[1], Alex Vermeulen[1,2], Wouter Peters[3,4]

[1]ICOS Carbon Portal at Lund University, Department of Physical Geography and Ecosystem Sciences, Lund, Sweden
[2]ICOS ERIC, Carbon Portal, Lund, Sweden
[3]Wageningen University, Environmental Sciences Group, Wageningen, The Netherlands
[4]University of Groningen, Centre for Isotope Research, Groningen, The Netherlands

Correspondence to: Ida Storm (ida.storm@nateko.lu.se)

Abstract. The ICOS (Integrated Carbon Observation System) network of atmospheric measurement stations produces standardized data on greenhouse gas concentrations at 36 stations in 14 different European countries (November 2022). The network targets a strongly heterogeneous landscape and the placement of instruments on tall towers and mountains make for large influence regions (footprints). The combined footprints for all the individual stations create the "lens" through which the observing network sees the European flux landscape. In this study, we summarize this view using quantitative metrics of the fluxes seen by individual stations, and by the current and future ICOS network. Results are presented both from a country-level and pan-European perspective, using open-source tools that we make available through the ICOS Carbon Portal. We target anthropogenic emissions from various sectors (e.g., energy production, industrial emissions), as well as the land-cover types found over Europe (e.g., broadleaf forests, croplands) and their spatiotemporally varying fluxes. This recognizes different interests of different ICOS stakeholders. We specifically introduce "monitoring potential maps", which quantify the sensitivity of the network with regards to specific properties of each pixel compared to the averages across all pixels, to see which regions have a relative underrepresentation of land-cover, or biospheric fluxes. This potential changes with the introduction of new stations, which we investigate for the planned ICOS expansion with 20 stations over the next few years. The monitoring potential concept is novel and a useful addition to traditional quantitative network design methods.

We find that the ICOS network has limited sensitivity to anthropogenic fluxes, as was intended in the current design. Its representation of biospheric fluxes follows the fractional representation of land-cover and is generally well balanced, with exceptions for a country like Norway where the southerly station Birkenes predominantly senses coniferous forest fluxes instead of the more abundant northerly grass & shrublands. Grass & shrubland fluxes are relatively underrepresented in ICOS, with the largest monitoring potential in Scandinavia, Croatia, and Serbia. These easterly countries similarly show a relative underrepresentation of broadleaf forest fluxes, partly due to a lack of monitoring stations, and partly due to the abundant sensitivity to broadleaf forests in the most densely monitored countries such as France and Germany. We stress that this does not imply these latter countries to be fully monitored and of lesser interest for network expansion: for example, inclusion of Schauinsland in the future network expands the network lens to mostly unmonitored mixed- and broadleaf forests which are

https://doi.org/10.5194/acp-2022-756
Preprint. Discussion started: 23 December 2022

Atmospheric Chemistry and Physics Discussions

relatively underrepresented at the national level. Such considerations demonstrate the usefulness of our analyses and can readily be re-produced for any network configuration within Europe with tools offered through the Carbon Portal.

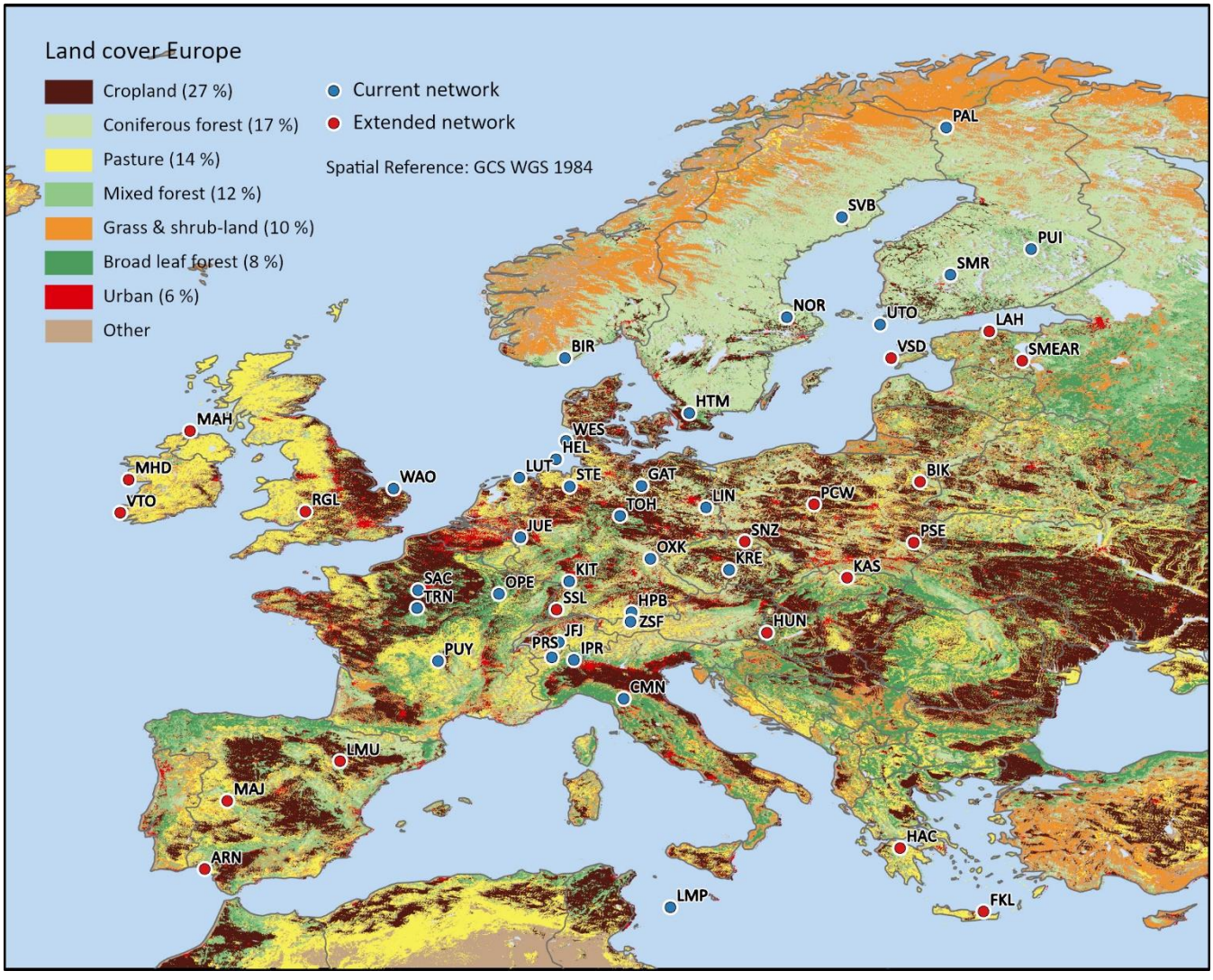

Figure 1: Current and prospective ICOS atmospheric stations within the STILT model domain (see Sect. 2.1). Main land cover classes are shown.

1 Introduction

Rising levels of carbon dioxide (CO_2) and its forcing towards a warmer climate have led 195 countries to sign the Paris Agreement, which was adopted in 2015. Countries committed to reduce their emissions and to review their commitments every five years in response to our common CO_2 trajectory. Up until now, about half of the CO_2 humans have emitted has been taken up by land (29% of total CO_2 emissions 2011-2020, Friedlingstein et al., 2022) or stored in the deep ocean (26% of total CO_2

https://doi.org/10.5194/acp-2022-756
Preprint. Discussion started: 23 December 2022


Atmospheric Chemistry and Physics Discussions

emissions 2011-2020, Friedlingstein et al., 2022). On global scale, our common CO_2 trajectory will greatly depend on the capacity for storage in these carbon reservoirs and is important to plan our efforts under the Paris agreement. Furthermore, understanding the natural carbon exchanges between carbon reservoirs is important for our ability to track and verify changes in emissions (Balsamo et al., 2021).

Our understanding of the carbon cycle has evolved over the last few decades, and atmospheric observations have been indispensable to gain deeper insights (Tans et al., 1990; Keeling et al., 2001; Francey et al., 1999; Bacastow et al., 1985). Long-standing records of direct CO_2 measurements, e.g. from Mauna Loa, Hawaii, famously show the increasing trend in global CO_2 levels (Sundquist and Keeling, 2009), and continue to form the basis of long-term analyses (Ballantyne et al., 2012; Graven et al., 2013; Liu et al., 2020). Additionally, inverse modelling systems have been employed at various scales to balance the atmospheric carbon budget, ensuring its consistency with observations from worldwide monitoring networks (Peylin et al., 2013; Thompson et al., 2016; Gaubert et al., 2019). Because of the relative uncertainty of biosphere fluxes compared to anthropogenic emissions, such studies have generally focused on exchange of CO_2 with the biosphere and oceans.

Measurements have traditionally been collected at remote islands, mountain tops, or other locations at large distance from direct emissions or uptake, to find well-mixed conditions that represent background atmospheric levels (Conway et al., 1994). Regional networks were added to this in the last two decades, with tall towers and aircraft data to inform on continental gradients in emissions and uptake (Sweeney et al., 2015; Turnbull et al., 2018) The European monitoring capacity is currently organized through the Integrated Carbon Observation System (ICOS; Heiskanen et al., 2021), a European infrastructure that provides standardized data on greenhouse gas concentrations in the atmosphere and fluxes between the atmosphere, land, and oceans. The ICOS network of atmospheric stations currently include 36 stations in 14 countries.

The measurements from the 36 ICOS atmospheric stations target a strongly heterogeneous flux landscape; Europe has multiple climate zones ranging from temperate with dry and hot summers in the South to cold Northern sub-Arctic climate without a dry season (Beck et al., 2018). The main land cover types are cropland, coniferous forest, pasture, mixed forest, grass & shrubland and broadleaf forest (see Fig. 1). Coniferous forests and grass & shrubland are prominent in the north, whereas the rest of Europe is more heterogeneous and generally has more cropland. Ecosystem management is strong across Europe, with land-use history, forest management, and cultivation of grasslands, croplands, and wetlands showing large differences from country to country. As a result of this heterogeneity, different ecosystems have different responses to climate anomalies, such as drought.

The network's ability to inform on the carbon cycle, such as responses to the 2018 drought (Peters et al., 2020; Ramonet et al., 2020), is directly tied to the influence areas ("footprints") of its stations. A station footprint represents where the air has passed on the way to the station for a specific point in time, and the carbon exchange in the footprint area is expected to influence the

https://doi.org/10.5194/acp-2022-756
Preprint. Discussion started: 23 December 2022


Atmospheric Chemistry and Physics Discussions

concentration at the station. Analyses of footprints to understand station and network representations have been exploited in previous studies. For example, Oney et al. (2015) used station footprints to analyse the suitability of a Swiss network of four stations for regional-scale carbon flux studies. A visual inspection of the average station footprints, and the expected signals associated with different land cover types, supported claims about where the monitoring can be expected to provide useful information. In Henne et al. (2010), footprints were analysed to classify stations based on expected representativeness of their measurements. Representative measurements have little or no influence from local emission sources, which make them appropriate for inclusion in regional inversion studies.

Previous network design studies also employed Quantitative Network Design (QND), where the impact of a given set of existing or hypothetical observations in a modeling framework is assessed to find an optimal network for a selected area of study (Kaminski and Rayner, 2017). The metric of how much value a potential station adds is typically the reduction in the assumed a-priori uncertainties of the carbon fluxes. QND often results in small networks targeting the largest signals, or on specific sources assumed least well-known. For example, in a QND study by Nickless et al. (2020) for Africa they found the optimal network to be focused on the productive region around the equator and that it changes with the seasons reflecting difference in flux activity and hence uncertainty. The chosen model set-up, the freedom to choose new station locations, and how the uncertainties are prescribed to the flux landscape thus has an influence on the results, and there is no fully objective quantification of optimal network design.

In this study, we therefore combine footprint analyses and quantification of sensing capacity in a different, yet quantitative approach. It focuses on what is seen by a station or network relative to the regional or national flux landscape, or relative to other stations, networks, or countries in Europe. Any underlying spatial data layer, ranging from population density to forest age or anthropogenic carbon emission, can be part of this quantification, recognizing that some fluxes, such as forests with high potential for long-term storage of carbon, might be more important than other. Our approach allows for a large flexibility in defining what makes for an appropriate station location, or an appropriate network, and allows expert judgement or formal optimization based on the outcomes.

We chose in this study to quantify and summarize the capacity of the ICOS atmospheric observing network to sense the underlying CO_2 flux landscape. We include anthropogenic fluxes as well as biospheric fluxes, and we discuss scales from individual stations, to countries, and to pan-European fluxes. Our main research goal is to identify areas with unexploited "monitoring potential", a novel concept that we introduce in this work. Areas with high monitoring potential would likely return useful information if targeted by expansion of the ICOS network. A secondary goal is to demonstrate the open-source tools we developed, to be used by a multitude of stakeholders, each with their own interest in the ICOS network, as available in the ICOS Carbon Portal. We describe our methods including how station and network footprints are created and combined with relevant data in Sect. 2. The first part of the results (3.1) focuses on the individual stations that make up the current and

https://doi.org/10.5194/acp-2022-756
Preprint. Discussion started: 23 December 2022


Atmospheric Chemistry and Physics Discussions

future ICOS network, followed by separate sections focused on what land-use types (3.2), and which fluxes (3.3) the network represents currently, and where important "monitoring potential" lies. The discussion (4) highlights limitations of the study and explain decisions that have influenced the results. The paper is concluded (5) with a summary.

2 Methods

2.1 Station footprints

Footprints are generated by STILT (Stochastic Time Inverted Lagrangian Transport; Lin et al., 2003), a Lagrangian atmospheric transport model. The extent of the footprints is limited to the model domain, i.e., 15°W-35°E and 33°N-73°N (the extent of Fig. 1). Output footprints are presented on a grid (1/12×1/8 degrees) with calculated surface influence ("sensitivity") in ppm / (µmol/ (m²s)). The sensitivities of the cells represent the station-specific atmospheric tracer dry mole fraction dependence on fluxes and are based on the dispersion of particles transported for ten days backward from the sampling time and location (x,y,z). Meteorological conditions drive the transport and are represented by three-hourly operational ECMWF-IFS analysis/forecasts. 10-day aggregated footprints are calculated for sampling times of every three hours (0:00, 3:00, 6:00, 9:00, 12:00, 15:00, 18:00, 21:00) and are available for download at the Carbon Portal (data.icos-cp.eu/) and viewing in the STILT viewer (https://stilt.icos-cp.eu/). The influence of using time-step aggregated footprints, also for the combination with biogenic fluxes, is deemed negligible for the purpose of our study.

2.2 Signals at the stations

Time-series of modelled CO_2 dry mole fraction and its components (i.e. individual anthropogenic- and biosphere-flux derived signals) are computed during the footprint calculation in the ICOS Carbon Portal tool. Footprints for hourly backward time-steps are combined with temporally resolved emissions and biogenic fluxes estimated in µmol/ (m²s). The EDGAR inventory (EDGARv4.3.2; Janssens-Maenhout et al., 2019; Gerbig and Koch, 2021b) is used for anthropogenic emissions and the VPRM biosphere model (Mahadevan et al., 2008; Gerbig, 2021a) for biogenic fluxes. Background mole fractions to account for the contributions from global fluxes are taken from the Jena CarboScope globally analysed atmospheric CO_2 fields (Rödenbeck and Heimann, 2021).

To relate the station derived biogenic signals to the latest high resolution land cover classification for Europe, alternative time-series for biosphere-flux derived signals have been created. The fluxes are combined with three-hourly time-step aggregated footprints (see Sect. 2.1) and attributed to different land cover types according to the HILDA (Winkler et al., 2020) land cover map. We specifically note that in the VPRM simulations the coarser SYNMAP (Jung et al., 2006) land cover map is used. The two maps represent land cover year 2018 and 2000 respectively.

https://doi.org/10.5194/acp-2022-756
Preprint. Discussion started: 23 December 2022


Atmospheric Chemistry and Physics Discussions

Ocean fluxes are currently not part of the STILT model set-up at the Carbon Portal. Rather, ocean fluxes from Carbon Tracker Europe-High Resolution (van der Woude et al., 2022b; van der Woude, 2022a) are combined with the three-hourly time-step aggregated footprints to create time-series of estimated ocean signals at the stations.

In case of multiple inlet heights at a station, the highest level is selected because the top-level measurements would have the largest footprints and are generally chosen to provide measurements for regional and global inverse modelling systems.

2.3 Station view of land cover

Summertime (JJA) and wintertime (JFD) average station footprints are combined with the HILDA land cover map to provide information of what land cover types are found within the footprint in different directions of the stations (see Fig. 2b). Attribution to land cover shares within individual countries is also possible by aggregating the footprints after masking with fractional country masks.

2.4 Network footprints

Two networks are considered in this study, the current ICOS network (see Fig. 4) and future ICOS network (see Fig. 8) which includes 20 stations that are expected to join the network in the next few years (see Fig.1). Three-hourly footprints for the individual stations in the network are reduced to cells with the highest sensitivity values that in combination add up to 50% of the sum of all cells. This follows the approach of Henne et al. (2010) and Oney et al. (2015) and is intended to emphasize areas with significant local influence. The footprints of the individual stations are combined in final three-hourly network footprints. Network footprints for the individual time-steps are needed as the biogenic flux maps have an hourly temporal resolution (see Sect. 2.5). In the case of multiple stations with sensitivity to the same footprint cell, the maximum cell value is used.

To estimate the overlap between a current network footprint and a footprint of a station that is included in the extended network, the effect of its inclusion in an updated network footprint is analysed; the difference between the spatial sums of the two network footprints are quantified and compared to the sum of the station footprint. If there is no overlap, the difference between the two network footprints is the same as the sum of the (50%) station footprint.

2.5 Network views of land cover and associated fluxes

Average summertime network footprints are combined with the HILDA land cover map to analyse what land cover types are sensed in individual countries and in Europe as a whole (referred to as “LC-view”). Fluxes associated with the different land cover classes are established from the combination of three-hourly network footprints with temporally corresponding flux map (referred to as “GEE-view”) and averaged for the summer. We use GEE rather than NEE as footprint-weight to prevent nearly cancelling photosynthesis and respiration signals to influence the network view. The GEE-view thus highlights areas with high biogenic activity. Areas of high biogenic activity are especially important to monitor because high activity generally means

https://doi.org/10.5194/acp-2022-756
Preprint. Discussion started: 23 December 2022


Atmospheric Chemistry and Physics Discussions

greater uncertainties in the current estimates and higher potential for long-term carbon storage. The network views are evaluated here exclusively for the summer when GEE is highest.

The LC- and GEE-views of the network are compared to what "equal views" would yield. An equal view is created by evenly distributing the sensitivity of network footprint cells within a region of interest and is used as a baseline to establish relative over- or underrepresentations of the LC-views and GEE-views. It should be noted that to have an "equal view" of the studied region is not always desirable as some fluxes might be more relevant to monitor than other. Consequently, over- and underrepresentations are not inherently negative for the network. Note that an equal LC-view reflects the relative distribution of area associated with different land cover types. In terms of the GEE-view, variations in the underlying biogenic fluxes of each land-cover mean that there can be over- and underrepresentation even if the relative shares are the same (see Fig. 5 and Fig. 7).

The following definitions are given to help the reader:

a: true network footprint (see Sect. 2.4)

b: equal view footprint

The total monitoring capacity of a network within a country or region is calculated by summarising the footprint cell values within its borders using masks. An equal share of the total is in turn assigned to all footprint cells to create an "equal view" footprint.

c: GEE flux map from VPRM

d: land-cover fractional mask

e: GEE-view

$$e = a * c * d \quad (1)$$

f: equal GEE-view

$$f = b * c * d \quad (2)$$

g: relative flux representation (used in Fig. 5b and Fig. 7b)

https://doi.org/10.5194/acp-2022-756
Preprint. Discussion started: 23 December 2022

Atmospheric Chemistry and Physics Discussions

$$g = \frac{sum(e)}{sum(f)} \quad (3)$$

The spatial difference in e and f signifies the over- or underrepresentation of a certain flux.

h: relative monitoring potential map (used in Sect. 3.2 and Sect. 3.3)

$$h = e - f \quad (4)$$

Cells where the equal view (f) is greater than the network view will have positive values in (h), and only these are displayed in the monitoring potential maps. Monitoring potential becomes especially high in areas where the current network is relatively blind, and the activity of the specific flux is relatively high. For the monitoring potential maps for the extended network, f is the same as for the current network. For monitoring potential within an individual country, a fractional country mask (0.0 is fully outside the border, 1.0 is fully within) is applied to (d) before the calculation of (e), (f), and (h).

3 Results

We focus the first part of the results (3.1) on characteristics of stations in the ICOS current and future networks and demonstrate our capacity for a deeper station analysis for Swedish station Hyltemossa. We then quantify how the monitoring network views the current European landscape in its current (3.2) and extended (3.3) ICOS configuration, with a focus on the new concept of "monitoring potential".

3.1 The view from individual stations

Station	Coniferous	Crop	Mixed forest	Pasture	Broad leaf	Urban	Grass & shrub	Other	Ocean	Energy	Transport	Industry	Residential
ARN100*	0.3	1.0	1.0	0.6	0.4	0.2	0.3	0.0	-0.01	0.4	0.4	0.2	0.1
BIK300*	2.4	4.5	1.7	1.7	1.2	0.7	1.2	0.1	-0.03	0.5	0.3	0.2	0.1
BIR075	5.2	1.1	0.8	0.5	0.3	0.2	0.6	0.2	-0.13	0.6	0.3	0.2	0.1
CMN760	1.1	2.3	1.5	1.3	4.2	0.9	0.7	0.1	-0.01	0.4	0.4	0.3	0.1
EST110*	2.9	2.7	3.6	0.8	1.7	0.3	1.6	0.3	-0.07	0.4	0.2	0.1	0.0
FKL015*	0.8	2.8	1.0	1.2	1.6	0.5	0.7	0.1	0.13	0.5	0.4	0.3	0.1
GAT344	1.9	3.9	1.1	1.3	0.5	0.8	0.5	0.1	-0.07	0.7	0.5	0.4	0.2
HAC*	1.0	2.9	1.3	1.8	2.1	0.5	0.8	0.1	0.01	0.4	0.3	0.2	0.1
HEL110	1.1	3.1	0.9	1.7	0.4	0.7	0.4	0.1	-0.09	0.6	0.4	0.3	0.1
HPB131	1.9	2.7	3.0	4.9	0.9	1.6	0.5	0.2	-0.03	0.5	0.7	0.4	0.2

https://doi.org/10.5194/acp-2022-756
Preprint. Discussion started: 23 December 2022

Atmospheric Chemistry and Physics Discussions

HTM150	3.0	2.8	1.6	0.7	0.9	0.4	0.5	0.2	-0.10	0.5	0.3	0.2	0.1
HUN115*	2.2	6.8	4.0	1.7	2.5	1.8	1.2	0.1	-0.03	0.7	0.7	0.5	0.2
IPR100	1.9	3.6	2.2	2.4	5.4	2.6	0.9	1.3	-0.01	0.8	1.6	1.7	0.5
JFJ	1.2	1.7	1.9	1.9	0.8	0.9	0.5	0.2	-0.02	0.3	0.4	0.2	0.1
JUE120	1.0	3.1	1.3	1.4	0.6	1.5	0.3	0.1	-0.07	5.6	1.1	1.3	0.5
KAS*	2.2	3.5	1.6	1.9	1.4	1.0	0.8	0.1	-0.02	0.6	0.4	0.3	0.1
KIT200	1.3	4.0	2.3	1.4	1.6	1.8	0.4	0.1	-0.05	1.6	0.8	0.7	0.3
KRE250	2.3	5.0	1.5	1.5	0.8	1.1	0.5	0.1	-0.04	0.7	0.5	0.4	0.2
LAH032*	5.0	2.2	3.3	0.8	1.0	0.4	1.4	0.3	-0.11	0.7	0.2	0.4	0.1
LIN099	3.0	4.0	1.3	1.3	0.6	1.0	0.7	0.1	-0.06	1.5	0.6	0.7	0.2
LMP	0.6	1.6	1.0	0.9	1.0	0.4	0.5	0.0	0.26	0.3	0.4	0.2	0.1
LMU080*	0.6	1.9	1.4	0.8	1.1	0.3	0.3	0.0	-0.03	0.3	0.4	0.2	0.1
LUT	1.1	4.2	0.9	2.3	0.4	1.0	0.4	0.3	-0.09	1.3	0.6	0.4	0.2
MAH*	0.8	0.9	0.6	1.9	0.2	0.3	0.3	0.1	-0.23	0.2	0.3	0.1	0.1
MAJ100*	0.4	0.9	1.2	1.1	0.5	0.2	0.3	0.0	-0.02	0.1	0.2	0.1	0.0
MHD*	0.5	0.8	0.4	1.4	0.1	0.2	0.6	0.2	-0.16	0.2	0.2	0.1	0.0
NOR100	5.7	1.8	1.6	0.3	0.2	0.2	0.5	0.3	-0.12	0.4	0.2	0.2	0.0
OPE120	0.8	3.4	1.1	1.1	1.4	0.8	0.2	0.1	-0.05	0.5	0.5	0.4	0.1
OXK163	2.2	3.4	1.5	1.5	0.8	1.2	0.4	0.1	-0.05	0.8	0.6	0.4	0.2
PAL	4.5	0.3	0.6	0.1	0.1	0.1	1.5	0.2	-0.10	0.1	0.1	0.1	0.0
PCW150*	2.1	5.7	1.4	1.6	0.8	0.9	1.0	0.1	-0.04	1.0	0.4	0.3	0.1
PRS	1.1	1.4	1.4	1.7	0.8	0.7	0.3	0.3	-0.02	0.2	0.3	0.2	0.1
PSE150*	2.7	5.1	1.9	2.0	1.3	1.5	1.3	0.1	-0.03	0.9	0.5	0.6	0.2
PUI084	5.0	0.8	2.1	0.2	0.3	0.1	0.5	0.6	-0.07	0.5	0.1	0.1	0.0
PUY	0.7	1.4	1.6	1.7	1.1	0.4	0.3	0.0	-0.03	0.2	0.3	0.2	0.1
RGL090*	0.6	2.3	0.8	2.0	0.2	0.6	0.3	0.1	-0.12	0.6	0.6	0.3	0.2
SAC100	0.6	2.9	0.7	0.9	0.8	0.8	0.2	0.1	-0.07	0.5	1.1	1.0	0.5
SMR125	5.9	1.3	1.6	0.3	0.3	0.2	0.5	0.5	-0.09	0.3	0.2	0.2	0.0
SNZ*	2.1	3.9	1.4	1.4	0.7	0.9	0.6	0.1	-0.04	0.7	0.4	0.3	0.1
SSL	1.4	2.9	2.2	1.5	1.3	1.3	0.3	0.1	-0.04	0.5	0.6	0.4	0.2
STE252	1.3	4.2	1.0	1.9	0.4	1.2	0.4	0.1	-0.08	1.0	0.6	0.5	0.2
SVB150	6.5	0.6	1.0	0.2	0.2	0.1	0.8	0.3	-0.10	0.2	0.1	0.1	0.0
TOH147	2.0	3.6	1.2	1.2	0.9	1.0	0.4	0.1	-0.06	0.9	0.6	0.6	0.2
TRN180	0.6	2.9	0.8	0.9	0.9	0.6	0.2	0.0	-0.06	0.3	0.5	0.3	0.2
UTO	3.6	1.6	1.6	0.4	0.5	0.2	0.6	0.2	-0.24	0.5	0.2	0.2	0.0
VSD006*	3.7	2.0	2.4	0.7	0.9	0.3	1.0	0.2	-0.29	0.4	0.2	0.2	0.0

https://doi.org/10.5194/acp-2022-756
Preprint. Discussion started: 23 December 2022

Atmospheric Chemistry and Physics Discussions

VTO014*	0.4	0.7	0.4	1.3	0.1	0.2	0.4	0.1	-0.06	0.2	0.2	0.1	0.1
WAO	0.9	4.8	0.8	1.4	0.2	0.8	0.4	0.2	-0.09	0.8	0.8	0.4	0.2
WES	1.2	3.7	1.0	1.7	0.3	0.7	0.5	0.2	-0.09	1.0	0.5	0.2	0.1
ZSF	2.0	2.0	1.9	2.4	0.8	1.0	0.5	0.2	-0.03	0.3	0.5	0.3	0.1

Table 1: Summertime (JJA) average land cover (GEE), anthropogenic, and ocean signals (ppm) at the stations in the current and extended (*) ICOS atmospheric networks. The GEE and ocean signals have been created using time-step aggregated footprints and should be used for qualitative analyses only (see Sect. 2.2.).

The individual stations of our studied networks show large variations in expected signals, with most stations larger in sensing capacity for biogenic fluxes than for anthropogenic emissions (Table 1). Considering sensitivity to biogenic activity, the highest average signal is associated with coniferous forests, followed by cropland. Coniferous forests are found in abundance in northern Europe and is associated with about 60% of the land area in some countries (see Fig. 1). This means large signals at Swedish Norunda (NOR100) and Svartberget (SVB150), and Finish SMEAR (SMR125) and Puijo (PUI084). Similarly, stations in countries with large areas associated with cropland, such as Czech Krésin (KRE250) and Dutch Lutjewad (LUT), show some of the largest signals associated with cropland. Although mole fraction contributions typically reflect land-cover fractions within the footprints, their ratios can vary over space and time due to variations in the underlying vegetation fluxes of each land-cover. For example, forests have normally higher photosynthetic activity than cropland which calls for the distinction between LC-view and GEE-view.

Signals from anthropogenic emissions are generally expected to be small because ICOS targets natural fluxes. For several stations, this targeting is proving successful and about one third of the stations have average anthropogenic signals below one ppm. These include several “background stations” with limited influence from local surface fluxes thanks to strategic placement by the ocean, including Lampedusa (LMP), Mace Head (MHD) and Malin Head (MAH), or on remote mountain tops, such as Jungfraujoch (JFJ), Plateau Rosa (PRS) and Puy de Dôme (PUY). However, high emission intensity in central European countries makes it hard to avoid significant emission sources within the large footprints of atmospheric stations. Generally, emissions related to energy production cause the largest signals, especially at German and Polish stations. However, it is important to remember that the signal averages include peaks in anthropogenic signals during particular hours especially when the wind transports air from large point source emitters. For example, German station Juelich (JUE) is located only 10 km from a coal-fired power plant that accounts for about 4% of Germany’s total emissions (E-PRTR) and whereas the average signal is 5.6 ppm, it is below 1.0 ppm about 20% of the time. Careful sub-sampling of time series, as suggested also by Oney et al. (2015), could allow for either avoiding anthropogenic influence or concentrating on its analysis. A deeper analysis per station is facilitated by our tools, as exemplified next for station Hyltemossa.

https://doi.org/10.5194/acp-2022-756
Preprint. Discussion started: 23 December 2022

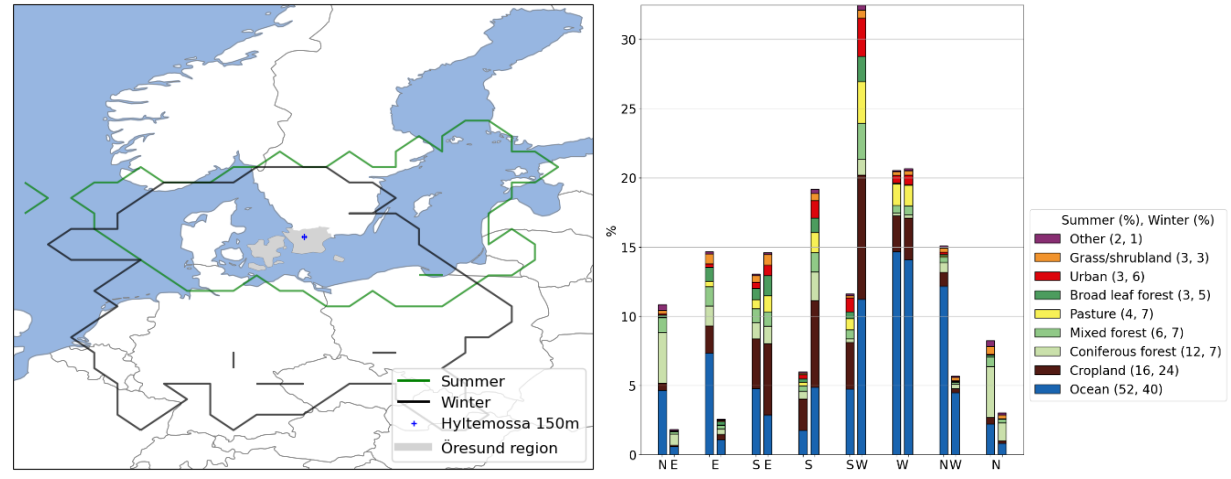

(a) (b)

Figure 2: (a) Hyltemossa's 50 % footprint area for summer and winter year 2020 (b) summer (JJA) and winter (JFD) land cover shares within the seasonal footprints split by direction.

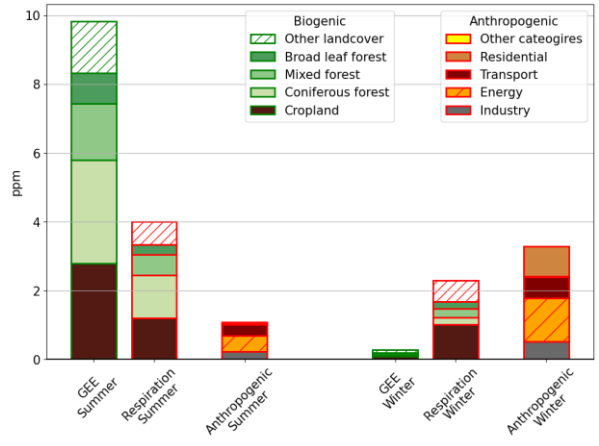

Figure 3: (a) Biogenic and anthropogenic signals at Hyltemossa, summer (JJA) and winter (JFD) 2020. The biogenic signals are attributed to different land cover types and the anthropogenic signals by source categories.

Hyltemossa is located in southern Sweden in an area of managed coniferous forests. Footprints calculated for the 150 meter inlet height are analysed, with major cities such as Malmo and Copenhagen well-within the large general footprint region (see Fig. 2a). The anthropogenic signals are nevertheless small, and it is an appropriate station for large-scale monitoring of oceanic and biospheric fluxes. Seasonal differences in footprints are substantial with larger footprints in the winter, extending south-west to an area characterized by more cropland and into densely populated regions such as the Oresund, Northern Germany, and the Netherlands. The size and extent of the average footprints for summer and winter can be further examined in Fig. 2a

https://doi.org/10.5194/acp-2022-756
Preprint. Discussion started: 23 December 2022

Atmospheric Chemistry and Physics Discussions

complemented by division of footprint sensitivity by land-cover in Fig. 2b. The summer footprint extends far east and west of the station, which explains the large share of sensitivity to ocean. Cropland has the second largest share within both the summer and winter footprints. Coniferous forest is the third most sensed land cover with a higher relative share in the summer because of favourable conditions for conifers mainly in the northern latitudes. Without analysis of the footprints, even higher sensing of coniferous forests would be expected with abundance in the vicinity of the station and in Sweden as a whole (60%).

The summertime atmospheric CO_2 signal at Hyltemossa strongly reflects the biospheric fluxes from the land-cover types under its footprint, but has the largest share of the signal associated with coniferous forest despite more cropland within the footprint (see Fig. 2b and Fig. 3). The coniferous forest flux signals mostly come from within Sweden's border (44% of GEE) while cropland signals at Hyltemossa originate from outside Sweden including Poland, Denmark, and Germany. During the winter, biosphere respiration of CO_2 is almost as large signal as the anthropogenic contribution, which is dominated by energy production, followed by residential. Interestingly, emission sources within Sweden only contribute about 10% of the anthropogenic signal at the station, and the previously mentioned Oresund region slightly more. The remainder is transported from emission sources further away, emphasizing the importance of long-range transport.

3.2 The view from the current ICOS network

We will start our analysis of the view from the current ICOS network by quantifying what land cover types are sensed by ICOS (3.2.1). The European scale view of the network is complemented with the view within individual countries to account for the uneven representation within Europe. A view of the fluxes associated with the different land cover types follows which is also used to produce monitoring potential maps (3.2.2).

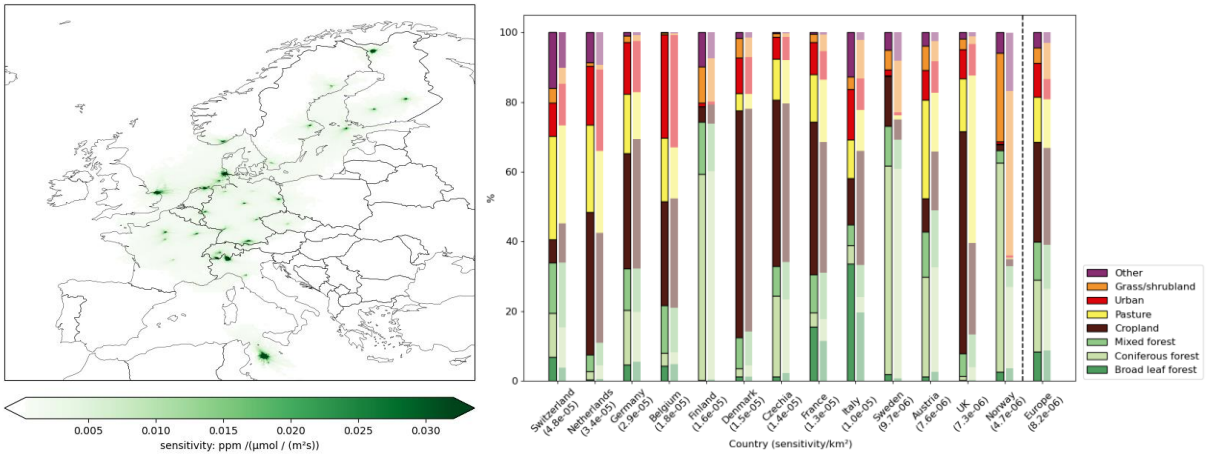

(a) (b)

https://doi.org/10.5194/acp-2022-756
Preprint. Discussion started: 23 December 2022

Atmospheric Chemistry and Physics Discussions

Figure 4: (a) Summer (JJA) 2020 network footprint. (b) sensitivity of network land cover (left bars) compared to country shares of land cover (right bars) in ICOS membership countries. The graph sorted from highest to lowest sensitivity per km^2 (values found in parentheses).

3.2.1 Land-cover types sensed by ICOS

The share of different land cover types within Europe is in general agreement with the shares of different land cover types sensed by the ICOS network, with main exceptions for an overrepresentation of coniferous forests and underrepresentation of grass & shrubland (see Fig. 4b, "Europe"). Results for the same type of analysis on the scale of the individual ICOS membership countries generally show larger differences for countries only partially within the average network footprint (see Fig. 4a). Coniferous forest is predominately sensed within the Scandinavian countries with network shares in Finland and Sweden matching their national shares, whereas Norway's only ICOS station is in an area abundant with coniferous forests which skews the network's sensing capacity. What is mainly missed is grass & shrubland which cover more than 40% of Norway's area. Other countries with high shares of grass & shrubland including Croatia, Serbia, and Albania are barely covered by footprints in the network and contribute to the relative underrepresentation on European scale. Broadleaf forests are fairly well represented on European scale but are relatively overrepresented in many of the ICOS membership countries including Italy, France, and Switzerland. Countries outside the network view with extensive areas of broadleaf forests, such as Slovakia and Slovenia, balance the local overrepresentation. This stresses the need for network-assessment on multiple scales, and for formal quantification to be complemented by a visual inspection of the network.

3.2.2 Fluxes sensed by ICOS

https://doi.org/10.5194/acp-2022-756
Preprint. Discussion started: 23 December 2022

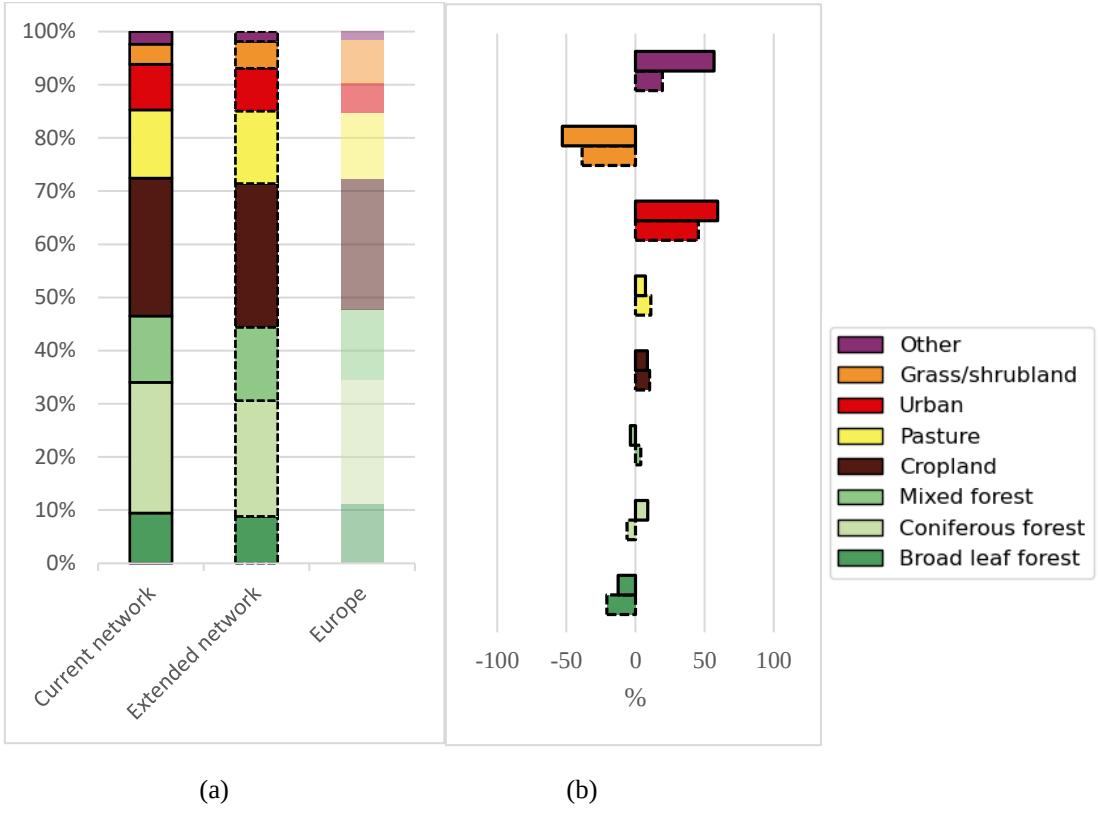

(a) (b)

Figure 5: (a) Share of flux (GEE) per land cover within Europe compared to the network GEE-view. (b) The over- (+) or under (-) representation of the ICOS network compared to an "equal view" of Europe (see Sect. 2.5).

305

When the GEE-view of the network is considered, network relative underrepresentation of broadleaf forest fluxes, in addition to grass & shrubland fluxes on European scale is revealed. The underrepresentation of broadleaf forest fluxes, despite a fair LC-view, means that broadleaf forests outside the focus of the network are relatively more active than those currently sensed. These active, relatively unmonitored forests are highlighted in a monitoring potential map (Fig. 6a) and indicates countries 310 outside the reach of the current network as high in potential, especially southeastern Europe. Within current ICOS membership countries, Italy shows great potential for broadleaf forest flux monitoring south of Monte Cimone (CMN) and, to lesser degrees, areas in southern France and eastern Czech Republic. Grass & shrubland is the most underrepresented flux and shows greatest potential for monitoring in Serbia and Croatia. Within the ICOS membership countries, Scandinavia has the highest potential.

https://doi.org/10.5194/acp-2022-756
Preprint. Discussion started: 23 December 2022

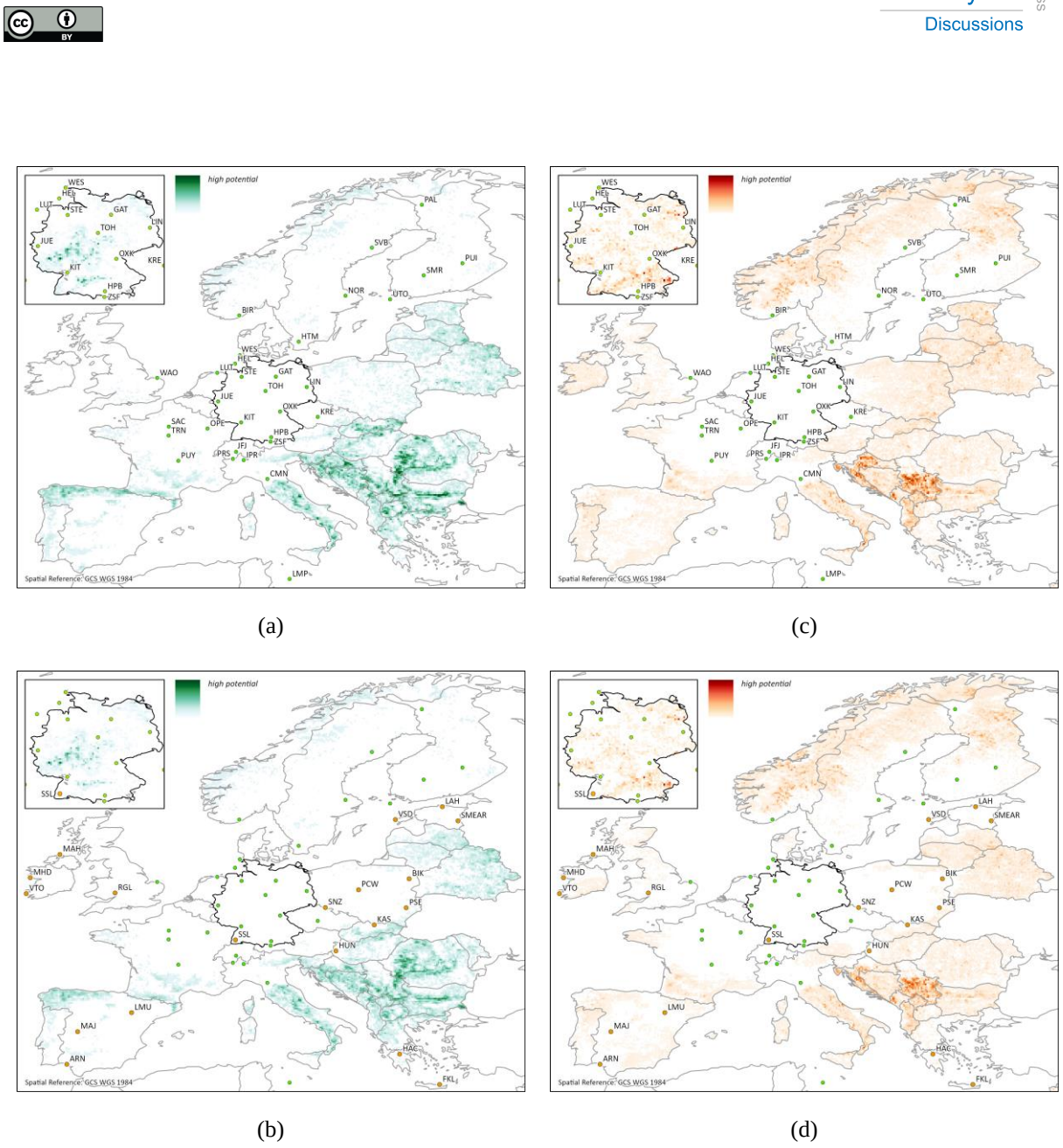

Figure 6: Monitoring potential of (a) broadleaf forest fluxes (GEE) for Europe and Germany (insert map) for the current and (b) extended ICOS networks (c) grass & shrubland fluxes (GEE) for Europe and Germany (insert map) for the current (d) extended ICOS network

The overrepresentation of sensing of fluxes associated with the land cover type urban, despite the ICOS network targeting natural fluxes, is explained by the relatively high density of stations in central Europe; countries with highest sensitivity per area unit (Switzerland, the Netherlands, and Germany) are also counties with some of the highest population densities. The relatively high sensing per unit area in central Europe also means that these countries show little or no monitoring potential on European scale. This should not be interpreted as if their monitoring is "complete"; it only means they are well-monitored

https://doi.org/10.5194/acp-2022-756
Preprint. Discussion started: 23 December 2022

Atmospheric Chemistry and Physics Discussions

relative to other areas in Europe. For expansion of national networks, the same approach can be employed on country scale to analyse flux representation and highlight relative monitoring potential which we will illustrate for Germany.

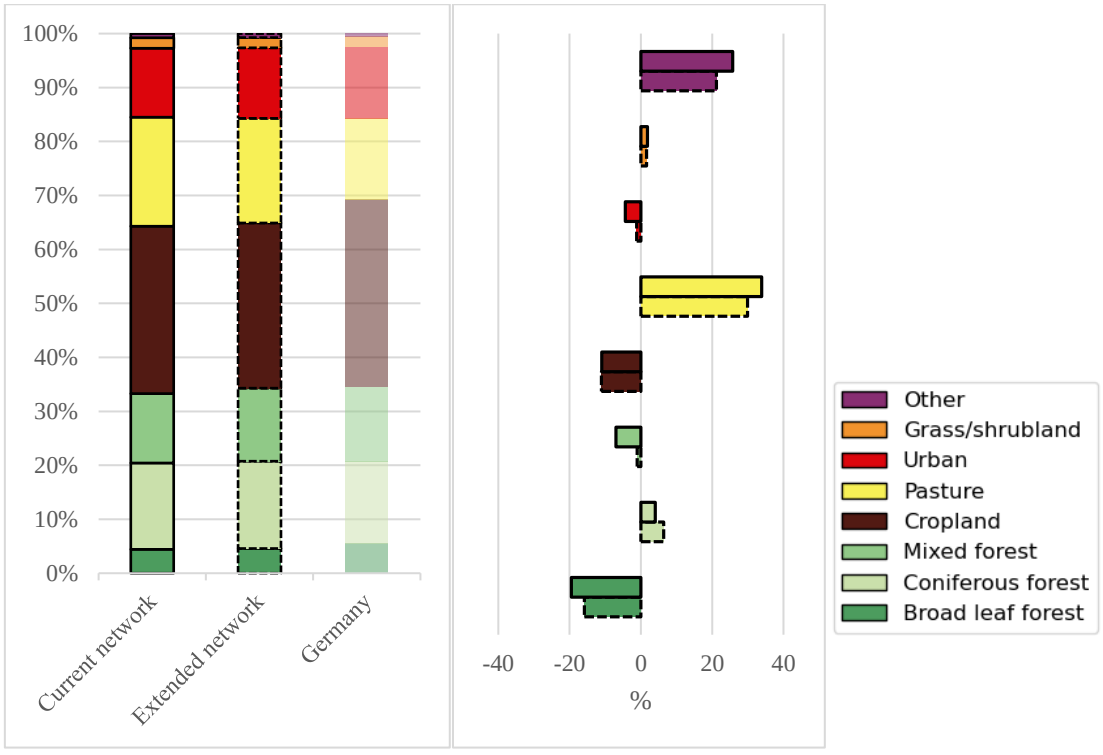

(a) (b)

Figure 7: (a) Share of flux (GEE) per land cover within Germany compared to the network GEE-view of Germany. (b) The over- or under- representation of the ICOS network compared to an "equal view" of Germany (see Sect. 2.5).

Germany is the ICOS member country with the largest number of atmospheric stations (ten) and has the third highest sensing capacity per area unit in Europe. Although the stations are spread throughout the country, the network represents some land cover fluxes better than other; broadleaf forest fluxes are relatively underrepresented also within Germany, with high monitoring potential in the central part of the country extending south to Karlsruhe (KIT) and west to Julich (JUE) (see Fig. 6a). However, broadleaf forests are only associated with 5% of the biogenic flux in Germany compared to 14% for mixed forests which is also underrepresented but to a lesser degree (see Table 3). Areas of high monitoring potential of the two forest types show a great deal of overlap but with mixed forests additionally having high potential in the south-eastern part of the country (not shown). The use of monitoring potential maps is not limited to underrepresented fluxes as demonstrated for relatively well-monitored grass & shrubland within Germany (see Fig. 6b). This is important because certain flux type might be targeted, and overrepresentation is in those cases desirable.

https://doi.org/10.5194/acp-2022-756
Preprint. Discussion started: 23 December 2022

Atmospheric Chemistry and Physics Discussions

3.3 The view from the extended ICOS network

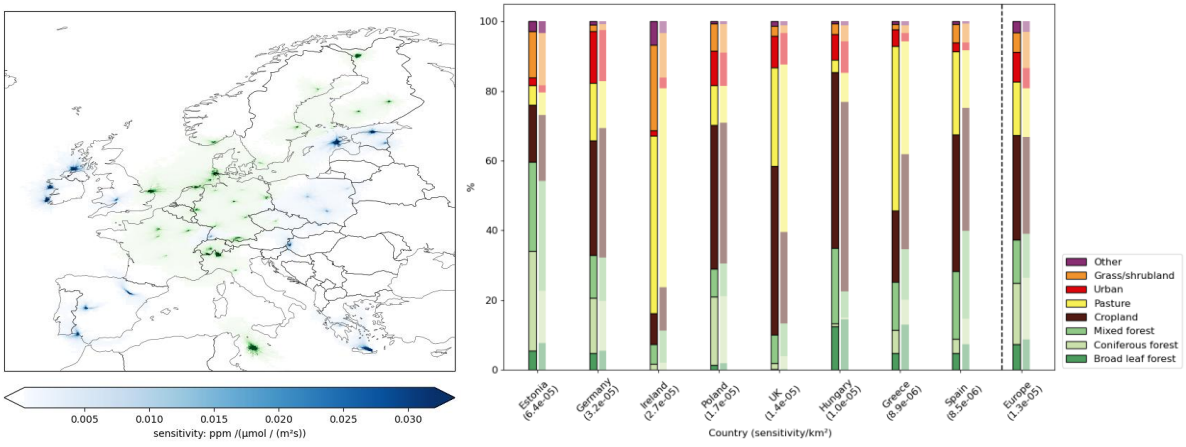

(a) (b)

345 **Figure 8: (a) Summer (JJA) 2020 extended network footprint. (b) Sensing of network to land cover (left bars) compared to country shares of land cover (right bars) in countries with stations added.**

The ICOS network is continuously expanding, and an additional 20 stations are expected to join in the next few years. This will greatly extend the reach of the network, especially as the planned stations are mainly sensitive to areas outside the focus
350 of the current network (see Fig. 8a). Overlap with the sensing capacity of the current network is close to zero for Spanish and Irish stations, and well-below 10% for all other added stations with exceptions for German Schauinsland (SSL) and Polish mountain-station Sněžka (SNZ). However, Schauinsland is added to a national network of ten other stations and the overlap is only 21%. This demonstrates the potential to fill network monitoring gaps also in relatively well-monitored countries. Whether the added stations make for a network with more equal representation of different land cover, and land cover associated fluxes
355 depends on the scale of the analysis. A fairer representation of land cover is evident at country level especially within countries previously without stations, whereas the representation on European scale show only small changes (see Fig. 8b). The difference in shares for Europe indicate that stations are added in areas of more cropland (particularly Polish stations, see Table 1) and pastures (particularly Irish, UK and Greek stations, see Table 1) than in coniferous forests. However, stations have yet to be added to areas with high monitoring potential of grass & shrubland (see fig. 5b) which is evident also by its continued
360 relative underrepresentation.

The flux-view similarly indicates a better representation within especially the previously unmonitored countries. On European scale, the extension will give a fairer network view if underrepresented fluxes are sensed more than the relative overrepresented

https://doi.org/10.5194/acp-2022-756
Preprint. Discussion started: 23 December 2022


Atmospheric Chemistry and Physics Discussions

fluxes. This is the case with mixed forest fluxes and to a lesser degree with grass & shrubland fluxes, whereas broadleaf forest fluxes are more underrepresented in the extended network. Figure 8 shows how the extended network improves the monitoring of broadleaf forests especially by the inclusion of the Hungarian station (HUN), but also that great monitoring potential in especially southeastern Europe remains. The extension of the German network with Schauinsland (SSL) in the south-western corner of the country especially improves the representation of mixed and broadleaf forest fluxes.

4 Discussion

This study offers an overview of the ICOS network's capacity to monitor the European carbon flux landscape by creating a lens with ICOS station footprints. Although the network includes stations in 14 European countries with extensive footprints that transect borders, there are several countries (e.g., Greece, Serbia, and Slovakia) to which the current network is blind. By contrasting the network view with an equal view of Europe and individual European countries, skewed representation of certain land cover types and land cover fluxes are exposed. Concentration of stations in central and northern Europe is favourable for monitoring especially cropland and coniferous forests, whereas the network is relatively blind to grass & shrubland fluxes. The footprint analysis is bridged with network design by providing a quantification through maps that highlight the greatest monitoring potential of individual flux types. On European scale, extensive areas in eastern and southeastern Europe are generally highlighted, whereas specific flux types still show great monitoring potential also within ICOS membership countries including broadleaf forests in southern Italy and grass & shrubland in Scandinavia.

The inclusion of prospective stations, partly in new member countries, greatly extends the spatial coverage of the network. This is a network that can better inform on the European carbon flux landscape, although the improved capacity does not necessarily mean increased representation by our definition where sensing everything equally is the baseline. For instance, the extended network still lacks stations in southeastern Europe which means a higher underrepresentation than in the current network. To plan for network expansion in relatively well-monitored countries, the scale should target a specific country, or even specific region within large countries. As exemplified with Germany, there are still monitoring gaps and unbalanced sensitivity across ecosystems even in member countries with many stations.

Our results are subject to uncertainties associated with the models we use for footprint calculation (STILT) and creation of biogenic flux maps (VPRM), as well as study-specific decisions. FLEXPART (Pisso et al., 2019) is a different footprint model that will be implemented at the Carbon Portal and will allow for comparisons and a choice for users of our tools. A study-specific decision is to create network footprints with station footprints that have been limited to the cells with highest influence that add up to 50% of the total sensitivity. This follows the approach of Henne et al. (2010) and Oney et al. (2015) and is intended to focus our work towards the strongest influence. In a sensitivity test, we also used the full station footprints (100%) and found our results robust for Europe, and for countries that have high shares of the network's monitoring capacity. Another

https://doi.org/10.5194/acp-2022-756
Preprint. Discussion started: 23 December 2022


Atmospheric Chemistry and Physics Discussions

choice was to use three-hourly footprints for summer (JJA) year 2020, with the assumption that they are generally applicable across our different years, stations, and networks. However, anomalous meteorology flow or extreme weather causing especially high or low photosynthetic activity could violate that assumption. Our focus on annual, or seasonal integrals mitigates this impact of anomalous footprints, but we did not test robustness against the choice of year at this stage.

The inlet height chosen for the footprint model is another aspect that impacts the final results. In case of multiple inlet heights at a station, the highest level was selected because the top-level measurements have the largest influence areas (footprints) and are generally chosen to provide measurements for regional and global inverse modelling systems. For stations with an air inlet close to the ground the sensitivity can be tenfold that of a mountain station. Signals at such low-inlet stations are generally larger and have in turn greater influence on resulting monitoring potential maps. This is an important aspect to keep in mind when new footprints are created and tested in networks. In our tools, users make their own decisions with regards to sensitivity threshold, study-period, and inlet height of stations.

In contrast to formal quantitative network design (QND) techniques, our approach does not suggest station locations for an optimal network. However, the metric for considering potential station location in QND studies is normally reduction of uncertainty of underlying carbon fluxes and tend to cluster around the station like footprints. In our approach, the footprints are not analysed in terms how uncertain the underlying fluxes are, but the derived monitoring potential maps will highlight areas where the highest under-monitored flux activity is. This normally coincides with where the prescribed uncertainties are highest in QND studies. Furthermore, the simplicity of our approach makes it possible to present Carbon Portal users with tools to consider any network configuration within Europe. The tools will be open for future development, and it will be possible to introduce new and updated data layers to overlay with the footprints as they become available or are found to be relevant by the community.

5 Conclusion

We evaluated the ICOS network to gain insight of what land cover types and land cover associated fluxes it represents to reveal strengths, weaknesses, and potential gaps. The network is formed by the combined views of the individual ICOS stations and has highest monitoring capacity in central and northern Europe where stations are relatively concentrated. The stations pick up signals throughout the heterogeneous European flux landscape and show a large variation of sensitivities, with generally larger sensing capacity for biogenic fluxes than for anthropogenic emissions. As a network, the land cover view relatively overrepresents coniferous forests and cropland as opposed to broadleaf forests and grass & shrubland on European scale. Country-scale considerations reveal a more uneven representation in some countries, such as Norway where coniferous forests are mainly within the network view. The land-cover view is not necessarily the same as the GEE-view due to CO_2-fluxes being spatially and temporally heterogeneous within European land-cover types and further indicates that highly active broadleaf

https://doi.org/10.5194/acp-2022-756
Preprint. Discussion started: 23 December 2022


Atmospheric Chemistry and Physics Discussions

forest fluxes are missed. Monitoring potential maps indicate especially high monitoring potential for this flux, and similarly underrepresented grass & shrubland flux, in southeastern Europe. The presented views of the carbon flux landscape from the ICOS network will change as new countries are joining the network, national networks are expanding, and the underlying flux landscape is changing. With careful planning of new station locations, we can hopefully make the most of measurements in the ongoing task of improving our understanding of the carbon flux landscape.

6 Code availability

A folder with scripts and a notebook to re-produce the analyses of the study also for other stations, countries, and networks has been published (Storm et al., 2022). There are dependencies with files on the ICOS Carbon Portal Jupyter Service (https://www.icos-cp.eu/data-services/tools/jupyter-notebook) and the notebook can only be run there. Hypothetical or actual stations with existing footprints can be used directly, and footprints for additional locations can be produced using the Carbon Portal's STILT on demand calculator (https://stilt.icos-cp.eu/viewer/).

7 Data availability

Datasets used as input for the analyses are listed throughout the paper. Station footprints used to create network footprints are published with persistent identifiers and available for download at the Carbon Portal (https://data.icos-cp.eu/). The figures and tables in the result section have been created with the published scripts.

Author contributions. IS, UK, AV, and WP designed the study. IS developed the Jupyter notebook package together with CD and UK. IS, WP, and UK prepared the paper, with contributions from all coauthors.

Competing interests. The authors declare that they have no conflict of interest.

References

Bacastow, R. B., Keeling, C. D., and Whorf, T. P.: Seasonal amplitude increase in atmospheric CO_2 concentration at Mauna Loa, Hawaii, 1959-1982, Journal of Geophysical Research: Atmospheres, 90, 10529–10540, https://doi.org/10.1029/jd090id06p10529, 1985.

Ballantyne, A. P., Alden, C. B., Miller, J. B., Tans, P. P., and White, J. W. C.: Increase in observed net carbon dioxide uptake by land and oceans during the past 50 years, Nature, 488, 70–72, https://doi.org/10.1038/nature11299, 2012.

Balsamo, G., Engelen, R., Thiemert, D., Agusti-Panareda, A., Bousserez, N., Broquet, G., Brunner, D., Buchwitz, M., Chevallier, F., Choulga, M., Denier Van Der Gon, H., Florentie, L., Haussaire, J.-M., Janssens-Maenhout, G., Jones, M. W.,

https://doi.org/10.5194/acp-2022-756
Preprint. Discussion started: 23 December 2022

Atmospheric Chemistry and Physics Discussions

Kaminski, T., Krol, M., Le Quéré, C., Marshall, J., McNorton, J., Prunet, P., Reuter, M., Peters, W., and Scholze, M.: The CO_2 Human Emissions (CHE) Project: First Steps Towards a European Operational Capacity to Monitor Anthropogenic CO_2 Emissions, Frontiers in Remote Sensing, 2, https://doi.org/10.3389/frsen.2021.707247, 2021.

Beck, H. E., Zimmermann, N. E., McVicar, T. R., Vergopolan, N., Berg, A., and Wood, E. F.: Present and future Köppen-Geiger climate classification maps at 1-km resolution, Scientific Data, 5, https://doi.org/10.1038/sdata.2018.214, 2018.

Conway, T. J., Tans, P. P., Waterman, L. S., Thoning, K. W., Kitzis, D. R., Masarie, K. A., and Zhang, N.: Evidence for interannual variability of the carbon cycle from the National Oceanic and Atmospheric Administration/Climate Monitoring and Diagnostics Laboratory Global Air Sampling Network, Journal of Geophysical Research, 99, 22831, https://doi.org/10.1029/94jd01951, 1994.

Francey, R. J., Allison, C. E., Etheridge, D. M., Trudinger, C. M., Enting, I. G., Leuenberger, M., Langenfelds, R. L., Michel, E., and Steele, L. P.: A 1000-year high precision record of $\delta^{13}C$ in atmospheric CO_2, Tellus - Series B, 51, 170 – 193, 1999.

Friedlingstein, P., Jones, M. W., O'Sullivan, M., Andrew, R. M., Bakker, D. C. E., Hauck, J., Quéré, C. L., Peters, G. P., Peters, W., Pongratz, J., Sitch, S., Canadell, J. G., Ciais, P., Jackson, R. B., Alin, S. R., Anthoni, P., Bates, N. R., Becker, M., Bellouin, N., Bopp, L., T. Chau, T. T., Chevallier, F., Chini, L. P., Cronin, M., Currie, K. I., Decharme, B., Djeutchouang, L. M., Dou, X., Evans, W., Feely, R. A., Feng, L., Gasser, T., Gilfillan, D., Gkritzalis, T., Grassi, G., Gregor, L., Gruber, N., Gürses, Ö., Harris, I., Houghton, R. A., Hurtt, G. C., Iida, Y., Ilyina, T., Luijkx, I. T., Jain, A., Jones, S. D., Kato, E., Kennedy, D., Goldewijk, K. K., Knauer, J., Korsbakken, J. I., Körtzinger, A., Landschützer, P., Lauvset, S. K., Lefèvre, N., Lienert, S., Liu, J., Marland, G., McGuire, P. C., Melton, J. R., Munro, D. R., Nabel, J. E. M. S., Nakaoka, S., Niwa, Y., Ono, T., Pierrot, D., Poulter, B., Rehder, G., Resplandy, L., Robertson, E., Rödenbeck, C., Rosan, T. M., Schwinger, J., Schwingshackl, C., Séférian, R., Sutton, A. J., Sweeney, C., Tanhua, T., Tans, P. P., Tian, H., Tilbrook, B., Tubiello, F., van der Werf, G. R., Vuichard, N., Wada, C., Wanninkhof, R., Watson, A. J., Willis, D., Wiltshire, A. J., Yuan, W., Yue, C., Yue, X., Zaehle, S., and Zeng, J.: Global Carbon Budget 2021, Earth System Science Data, 14, 1917–2005, https://doi.org/10.5194/essd-14-1917-2022, 2022.

Gaubert, B., Stephens, B. B., Basu, S., Chevallier, F., Deng, F., Kort, E. A., Patra, P. K., Peters, W., Rödenbeck, C., Saeki, T., Schimel, D., der Laan-Luijkx, I. V., Wofsy, S., and Yin, Y.: Global atmospheric CO_2 inverse models converging on neutral tropical land exchange, but disagreeing on fossil fuel and atmospheric growth rate, Biogeosciences, 16, 117–134, https://doi.org/10.5194/bg-16-117-2019, 2019.

Gerbig, C.: Parameters for the Vegetation Photosynthesis and Respiration Model VPRM (Version 1.1), ICOS-ERIC – Carbon Portal [data set], https://doi.org/10.18160/R9X0-BW7T, 2021a.

Gerbig, C., and Koch, F.-T.: European anthropogenic CO_2 emissions based on EDGARv4.3 and BP statistics 2021 for 2005-2020 (Version 1.0), ICOS ERIC – Carbon Portal [data set], https://doi.org/10.18160/2M77-62E6, 2021b.

Graven, H. D., Keeling, R. F., Piper, S. C., Patra, P. K., Stephens, B. B., Wofsy, S. C., Welp, L. R., Sweeney, C., Tans, P. P., Kelley, J. J., Daube, B. C., Kort, E. A., Santoni, G. W., and Bent, J. D.: Enhanced Seasonal Exchange of CO_2 by Northern Ecosystems Since 1960, Science, 341, 1085–1089, https://doi.org/10.1126/science.1239207, 2013.

Heiskanen, J., Brümmer, C., Buchmann, N., Calfapietra, C., Chen, H., Gielen, B., Gkritzalis, T., Hammer, S., Hartman, S., Herbst, M., Janssens, I. A., Jordan, A., Juurola, E., Karstens, U., Kasurinen, V., Kruijt, B., Lankreijer, H., Levin, I., Linderson, M., Loustau, D., Merbold, L., Myhre, C. L., Papale, D., Pavelka, M., Pilegaard, K., Ramonet, M., Rebmann, C., Rinne, J., Rivier, L., Saltikoff, E., Sanders, R., Steinbacher, M., Steinhoff, T., Watson, A., Vermeulen, A. T., Vesala, T., Vitkova, G., and Kutsch, W.: The Integrated Carbon Observation System in Europe, Bulletin of the American Meteorological Society, pp. 1–54, https://doi.org/10.1175/bams-d-19-0364.1, 2021.

Henne, S., Brunner, D., Folini, D., Solberg, S., Klausen, J., and Buchmann, B.: Assessment of parameters describing representativeness of air quality in-situ measurement sites, Atmospheric Chemistry and Physics, 10, 3561–3581, https://doi.org/10.5194/acp-10-3561-2010, 2010.

Janssens-Maenhout, G., Crippa, M., Guizzardi, D., Muntean, M., Schaaf, E., Dentener, F., Bergamaschi, P., Pagliari, V., Olivier, J. G. J., Peters, J. A. H. W., van Aardenne, J. A., Monni, S., Doering, U., Petrescu, A. M. R., Solazzo, E., and Oreggioni, G. D.: EDGAR v4.3.2 Global Atlas of the three major greenhouse gas emissions for the period 1970–2012, Earth System Science Data, 11, 959–1002, https://doi.org/10.5194/essd-11-959-2019, 2019.

Jung, M., Henkel, K., Herold, M., and Churkina, G.: Exploiting synergies of global land cover products for carbon cycle modeling, Remote Sensing of Environment, 101, 534–553, https://doi.org/10.1016/j.rse.2006.01.020, 2006.

Kaminski, T. and Rayner, P. J.: Reviews and syntheses: guiding the evolution of the observing system for the carbon cycle through quantitative network design, Biogeosciences, 14, 4755–4766, https://doi.org/10.5194/bg-14-4755-2017, 2017.

Keeling, C. D., Piper, S. C., Bacastow, R. B., Wahlen, M., Whorf, T. P., Heimann, M., and Meijer, H. A.: Exchanges of Atmospheric CO_2 and $^{13}CO_2$ with the Terrestrial Biosphere and Oceans from 1978 to 2000. I. Global Aspects., UC San Diego: Scripps Institution of Oceanography, 2001.

Lin, J. C., Gerbig, C., Wofsy, S. C., Andrews, A. E., Daube, B. C., Davis, K. J., and Grainger, C. A.: A near-field tool for simulating the upstream influence of atmospheric observations: The Stochastic Time-Inverted Lagrangian Transport (STILT) model, Journal of Geophysical Research, 108, ACH 2–1–ACH 2–17, https://doi.org/10.1029/2002jd003161, 2003.

Liu, Z., Ciais, P., Deng, Z., Lei, R., Davis, S. J., Feng, S., Zheng, B., Cui, D., Dou, X., Zhu, B., Guo, R., Ke, P., Sun, T., Lu, C., He, P., Wang, Y., Yue, X., Wang, Y., Lei, Y., Zhou, H., Cai, Z., Wu, Y., Guo, R., Han, T., Xue, J., Boucher, O., Boucher, E., Chevallier, F., Tanaka, K., Wei, Y., Zhong, H., Kang, C., Zhang, N., Chen, B., Xi, F., Liu, M., Bréon, F.-M., Lu, Y., Zhang, Q., Guan, D., Gong, P., Kammen, D. M., He, K., and Schellnhuber, H. J.: Near-real-time monitoring of global CO_2 emissions reveals the effects of the COVID-19 pandemic, Nature Communications, 11, https://doi.org/10.1038/s41467-020-18922-7, 2020.

Mahadevan, P., Wofsy, S. C., Matross, D. M., Xiao, X., Dunn, A. L., Lin, J. C., Gerbig, C., Munger, J. W., Chow, V. Y., and Gottlieb, E. W.: A satellite-based biosphere parameterization for net ecosystem CO_2 exchange: Vegetation Photosynthesis and Respiration Model (VPRM), Global Biogeochemical Cycles, 22, https://doi.org/10.1029/2006gb002735, 2008.

Nickless, A., Scholes, R. J., Vermeulen, A., Beck, J., Lopez-Ballesteros, A., Ardö, J., Karstens, U., Rigby, M., Kasurinen, V., Pantazatou, K., Jorch, V., and Kutsch, W.: Greenhouse gas observation network design for Africa, Tellus B: Chemical and Physical Meteorology, 72, 1–30, https://doi.org/10.1080/16000889.2020.1824486, 2020.

Oney, B., Henne, S., Gruber, N., Leuenberger, M., Bamberger, I., Eugster, W., and Brunner, D.: The CarboCount CH sites: characterization of a dense greenhouse gas observation network, Atmospheric Chemistry and Physics, 15, 11 147–11 164, https://doi.org/10.5194/acp-15-11147-2015, 2015.

Peters, W., Bastos, A., Ciais, P., and Vermeulen, A.: A historical, geographical and ecological perspective on the 2018 European summer drought, Philosophical Transactions of the Royal Society B: Biological Sciences, 375, 20190505, https://doi.org/10.1098/rstb.2019.0505, 2020.

Peylin, P., Law, R. M., Gurney, K. R., Chevallier, F., Jacobson, A. R., Maki, T., Niwa, Y., Patra, P. K., Peters, W., Rayner, P. J., Rödenbeck, C., van der Laan-Luijkx, I. T., and Zhang, X.: Global atmospheric carbon budget: results from an ensemble of atmospheric CO_2 inversions, Biogeosciences, 10, 6699–6720, https://doi.org/10.5194/bg-10-6699-2013, 2013.

https://doi.org/10.5194/acp-2022-756
Preprint. Discussion started: 23 December 2022


Atmospheric Chemistry and Physics Discussions

Pisso, I., Sollum, E., Grythe, H., Kristiansen, N. I., Cassiani, M., Eckhardt, S., Arnold, D., Morton, D., Thompson, R. L., Zwaaftink, C. D. G., Evangeliou, N., Sodemann, H., Haimberger, L., Henne, S., Brunner, D., Burkhart, J. F., Fouilloux, A., Brioude, J., Philipp, A., Seibert, P., and Stohl, A.: The Lagrangian particle dispersion model FLEXPART version 10.4, Geoscientific Model Development, 12, 4955–4997, https://doi.org/10.5194/gmd-12-4955-2019, 2019.

Ramonet, M., Ciais, P., Apadula, F., Bartyzel, J., Bastos, A., Bergamaschi, P., Blanc, P. E., Brunner, D., di Torchiarolo, L. C., Calzolari, F., Chen, H., Chmura, L., Colomb, A., Conil, S., Cristofanelli, P., Cuevas, E., Curcoll, R., Delmotte, M., di Sarra, A., Emmenegger, L., Forster, G., Frumau, A., Gerbig, C., Gheusi, F., Hammer, S., Haszpra, L., Hatakka, J., Hazan, L., Heliasz, M., Henne, S., Hensen, A., Hermansen, O., Keronen, P., Kivi, R., Komínková, K., Kubistin, D., Laurent, O., Laurila, T., Lavric, J. V., Lehner, I., Lehtinen, K. E. J., Leskinen, A., Leuenberger, M., Levin, I., Lindauer, M., Lopez, M., Myhre, C. L., Mammarella, I., Manca, G., Manning, A., Marek, M. V., Marklund, P., Martin, D., Meinhardt, F., Mihalopoulos, N., Mölder, M., Morgui, J. A., Necki, J., O'Doherty, S., O'Dowd, C., Ottosson, M., Philippon, C., Piacentino, S., Pichon, J. M., Plass-Duelmer, C., Resovsky, A., Rivier, L., Rodó, X., Sha, M. K., Scheeren, H. A., Sferlazzo, D., Spain, T. G., Stanley, K. M., Steinbacher, M., Trisolino, P., Vermeulen, A., Vítková, G., Weyrauch, D., Xueref-Remy, I., Yala, K., and Kwok, C. Y.: The fingerprint of the summer 2018 drought in Europe on ground-based atmospheric CO_2 measurements, Philosophical Transactions of the Royal Society B: Biological Sciences, 375, 20190513, https://doi.org/10.1098/rstb.2019.0513, 2020.

Rödenbeck, C. and Heimann, M.: Jena CarboScope: Atmospheric CO_2 inversion, Max Planck Institute for Biogeochemistry, Jena [data set], https://doi.org/10.17871/CarboScope-s10oc_v2021, 2021.

Storm, I., Karstens, U., D'Onofrio, C.: Network view notebook tool, ICOS RI, https://meta.icos-cp.eu/objects/33Y2PFeaaetgzj2rrQECP1dF, 2022.

Sundquist, E. T. and Keeling, R. F.: The Mauna Loa carbon dioxide record: Lessons for long-term Earth observations, in: Carbon Sequestration and Its Role in the Global Carbon Cycle, pp. 27– 35, American Geophysical Union, https://doi.org/10.1029/2009gm000913, 2009.

Sweeney, C., Karion, A., Wolter, S., Newberger, T., Guenther, D., Higgs, J. A., Andrews, A. E., Lang, P. M., Neff, D., Dlugokencky, E., Miller, J. B., Montzka, S. A., Miller, B. R., Masarie, K. A., Biraud, S. C., Novelli, P. C., Crotwell, M., Crotwell, A. M., Thoning, K., and Tans, P. P.: Seasonal climatology of CO_2 across North America from aircraft measurements in the NOAA/ESRL Global Greenhouse Gas Reference Network, Journal of Geophysical Research: Atmospheres, 120, 5155–5190, https://doi.org/10.1002/2014jd022591, 2015.

https://doi.org/10.5194/acp-2022-756
Preprint. Discussion started: 23 December 2022

Atmospheric Chemistry and Physics Discussions

Tans, P. P., Fung, I. Y., and Takahashi, T.: Observational Contrains on the Global Atmospheric CO_2 Budget, Science, 247, 1431–1438, https://doi.org/10.1126/science.247.4949.1431, 1990.

595 Thompson, R. L., Patra, P. K., Chevallier, F., Maksyutov, S., Law, R. M., Ziehn, T., van der Laan-Luijkx, I. T., Peters, W., Ganshin, A., Zhuravlev, R., Maki, T., Nakamura, T., Shirai, T., Ishizawa, M., Saeki, T., Machida, T., Poulter, B., Canadell, J. G., and Ciais, P.: Top-down assessment of the Asian carbon budget since the mid 1990s, Nature Communications, 7, https://doi.org/10.1038/ncomms10724, 2016.

600 Turnbull, J. C., Karion, A., Davis, K. J., Lauvaux, T., Miles, N. L., Richardson, S. J., Sweeney, C., McKain, K., Lehman, S. J., Gurney, K. R., Patarasuk, R., Liang, J., S., P. B., Heimburger, A., Harvey, R., and Whetstone, J.: Synthesis of Urban CO_2 Emission Estimates from Multiple Methods from the Indianapolis Flux Project (INFLUX), Environmental Science & Technology, 53, 287–295, https://doi.org/10.1021/acs.est.8b05552, 2018.

605 van der Woude, A. M.: Near real time fluxes (Version 0.5), ICOS ERIC – Carbon Portal [data set], https://doi.org/10.18160/20Z1-AYJ2, 2022a.

van der Woude, A. M., de Kok, R., Smith, N., Luijkx, I. T., Botia, S., Karstens, U., Kooijmans, L. M. J., Koren, G., Meijer, H., Steeneveld, G.-J., Storm, I., Super, I., Scheeren, B. A., Vermeulen, A., and Peters, W.: Near real-time CO_2 fluxes from
610 CarbonTracker Europe for high resolution atmospheric modeling, Atmospheric Chemistry and Physics [preprint], https://doi.org/10.5194/essd-2022-175, May 22 2022b.

Winkler, K., Fuchs, R., Rounsevell, M.: HILDA+ Global Land Use Change between 1960 and 2019, PANGAEA [data set], https://doi.org/10.1594/PANGAEA.921846, 2020.